Vector Magnetic Tomography: application to magnetic nanostructures and singularities

S. Ferrer

Outline

- Introduction
- Mistral beamline : soft X ray microscope
- Tomographic reconstruction method
- Experimental results
- Topological charges and emergent magnetic field
- Bloch dipoles and triplets in a permalloy sample
- Hyperbolic Bloch points in ferrimagnetic exchange spring
- Conclusions and additional considerations

Introduction

- Nanomagnetism is at present the most active area of research of magnetism that was initiated 1988 with the Giant Magnetoresistance effect in multilayers of Fe/Cr stacks

- Spintronics is based on the magnetism of engineered stacks of multilayers of magnetic (ferro and antiferromagnets) and non magnetic layers as metals or insulators. Multilayer technology is the basis of most magnetic storage media specially hard disk drivers.

- Several breakthroughs in the last decades are:

  1995 tunnel magnetoresistance involving spin dependent tunneling through an insulating layer

  1996 spin transfer torque that allows to manipulate the magnetization by a spin polarized current leading to the proposal of current induced domain wall motion along race tracks

2009 observation of the Dzyaloshinskii-Moriya asymmetric exchange interaction which favors canting of the magnetization and allows to rationalize chiral magnetic structures and magnetic singularities

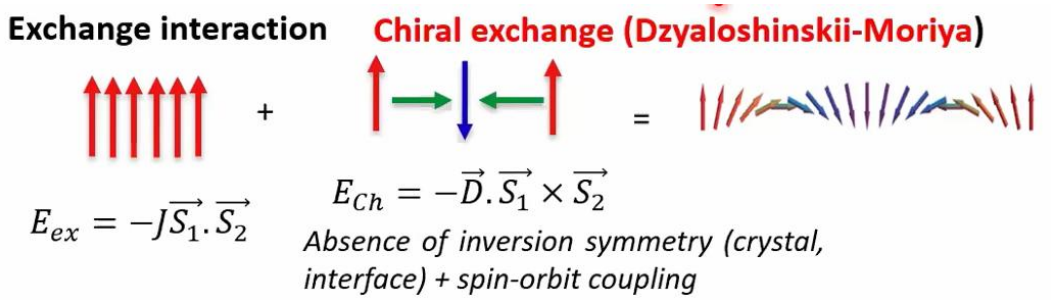

2009

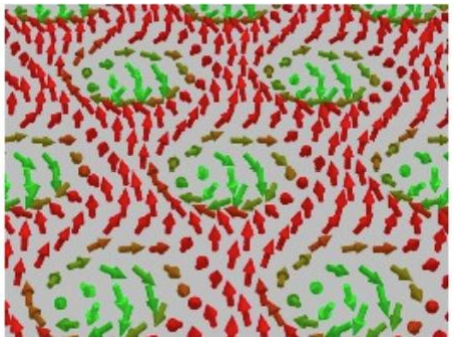

Skrmion lattice in MnSi

***SCIENCE* 323,** Iss 5916 pp. 915 (2009)

2009

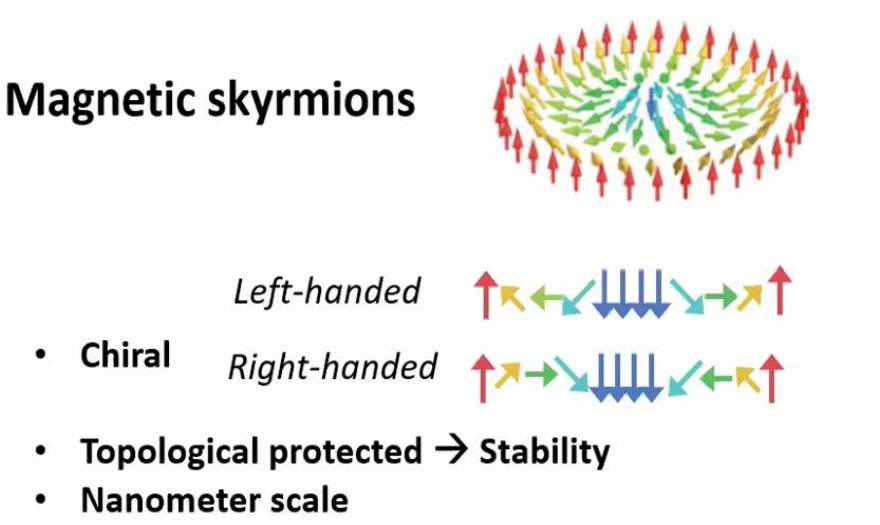

2013

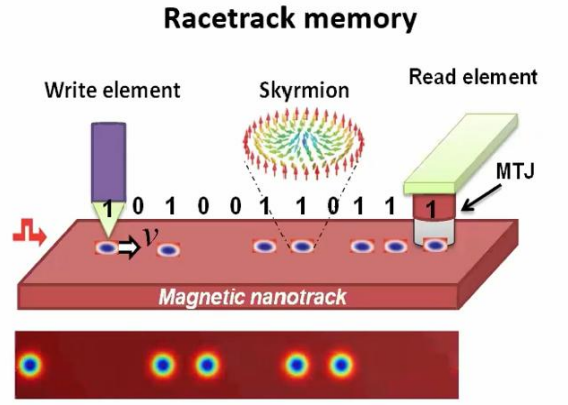

- Dzyaloshinskii-Moriya coupling and skyrmions have stimulated interest on on stable topological magnetic entities leading to a detailed understanding of magnetic singularities including several new concepts as the topological charge.

- Most of the previous works involve two-dimensional planar structures, however, recent work is expanding nanomagnetism into three dimensions a move triggered by the advance of unconventional synthesis methods and the discovery of new magnetic effects. In three-dimensional nanomagnets more complex magnetic configurations become possible, many with unprecedented properties

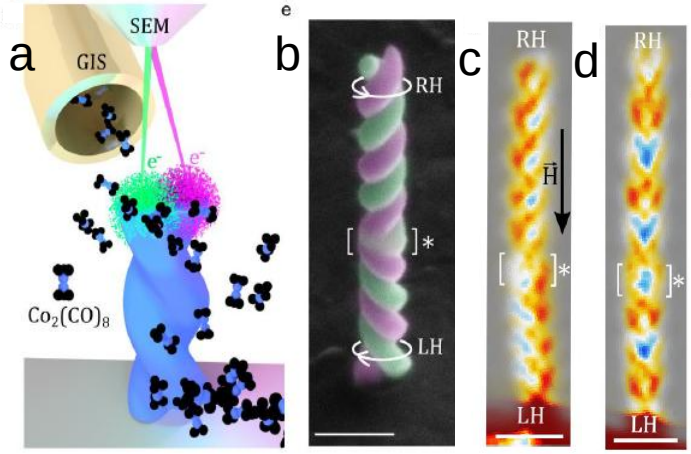

200 nm

ACS Nano **2020** *14* (7), 8084-809

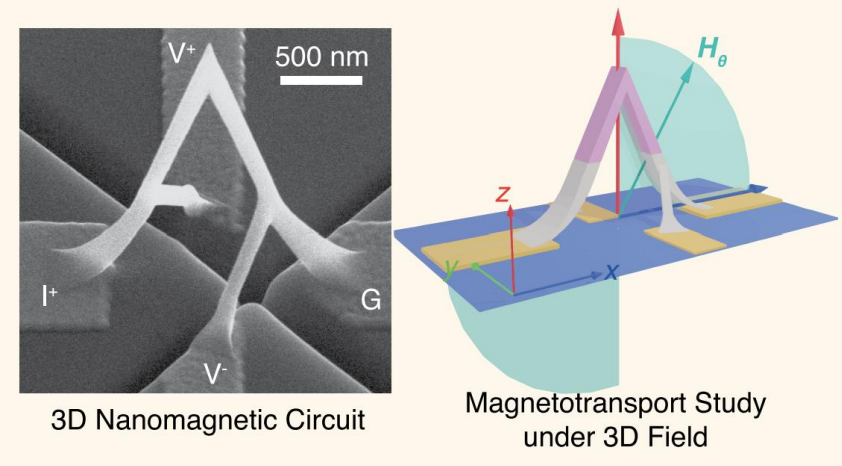

ACS Nano **2021**, 15, 6765−6773

- Most imaging techniques to visualize magnetic configurations have been surface sensitive (STM, PEEM….) well suited for 2D magnetic systems as interfaces or multilayers. They have been used in combination with micromagnetic simulations

- 3D nanomagnetism requires 3D visualization techniques. Some results have been achieved with Lorentz-TEM but the natural choice is tomography.

- Pionering work has been done at SLS with hard X rays and ptychography

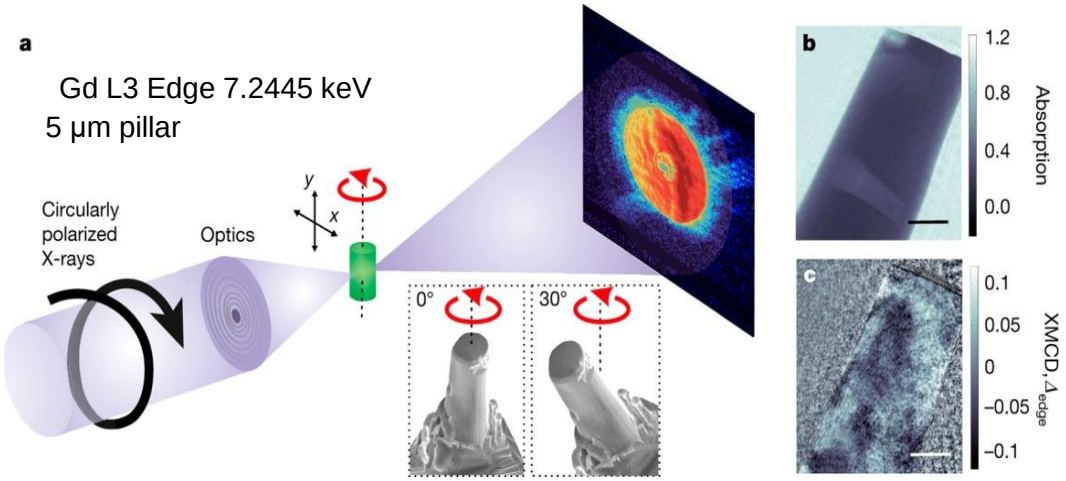

Nature **547,** 328–331 (2017) doi:10.1038/nature23006

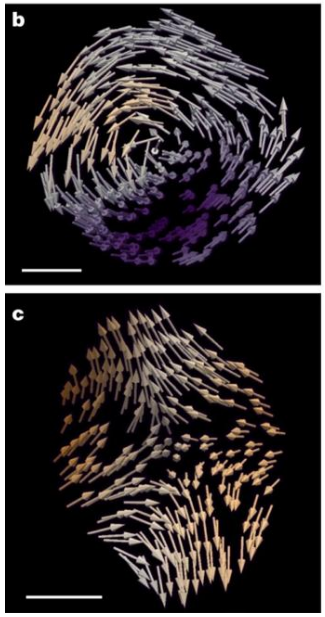

scale bar 300 nm

At ALBA we have developed vectorial tomography with soft X rays at the X ray microscopy beamline MISTRAL

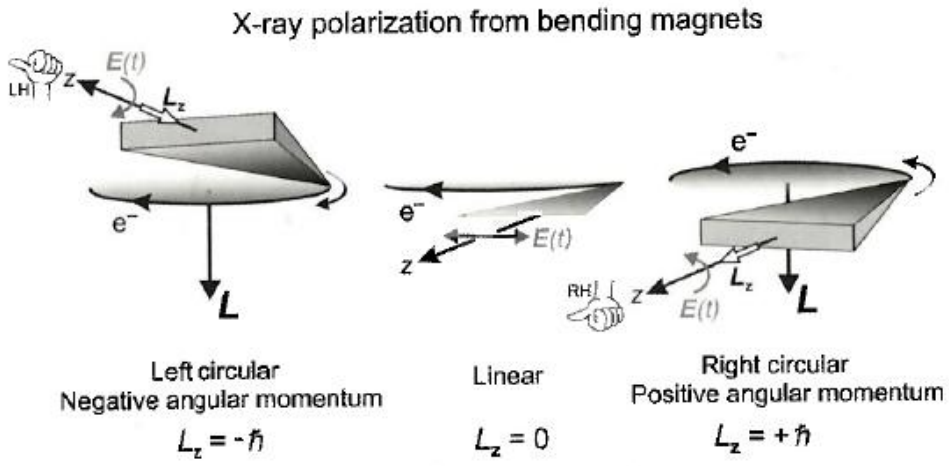

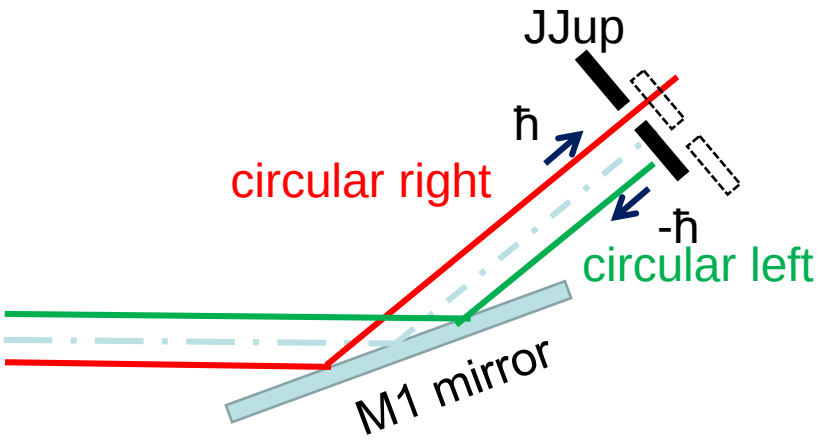

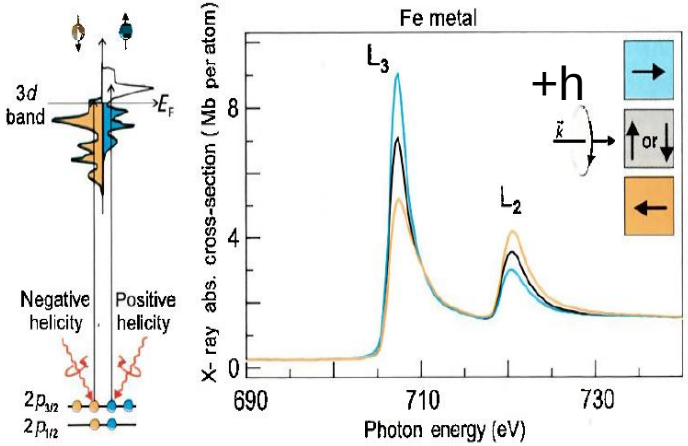

MISTRAL Beamline: X ray microscopy

optics

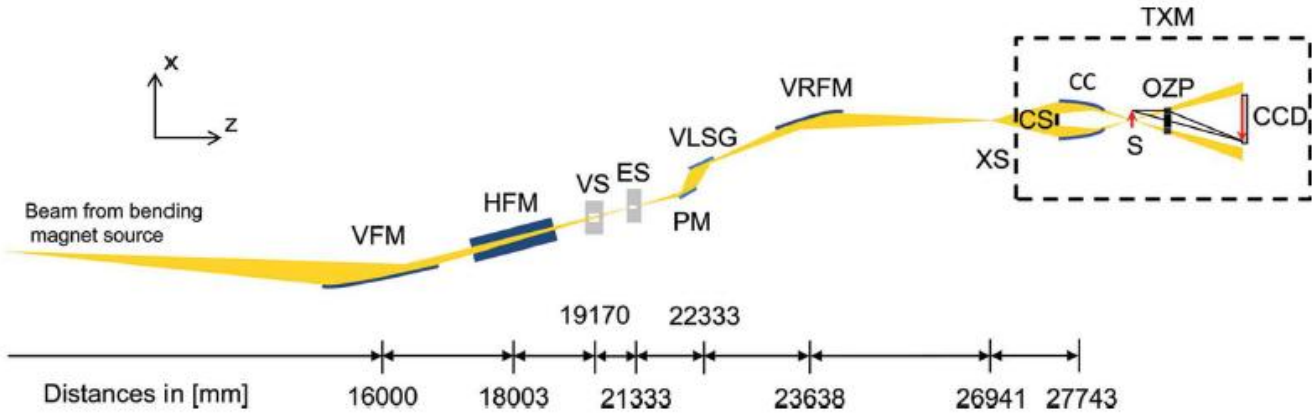

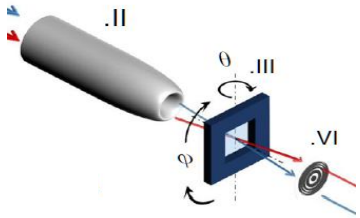

the inside…

working conditions: ZP @ 0.8-1.5 mm & condenser @ 9.5 mm from sample

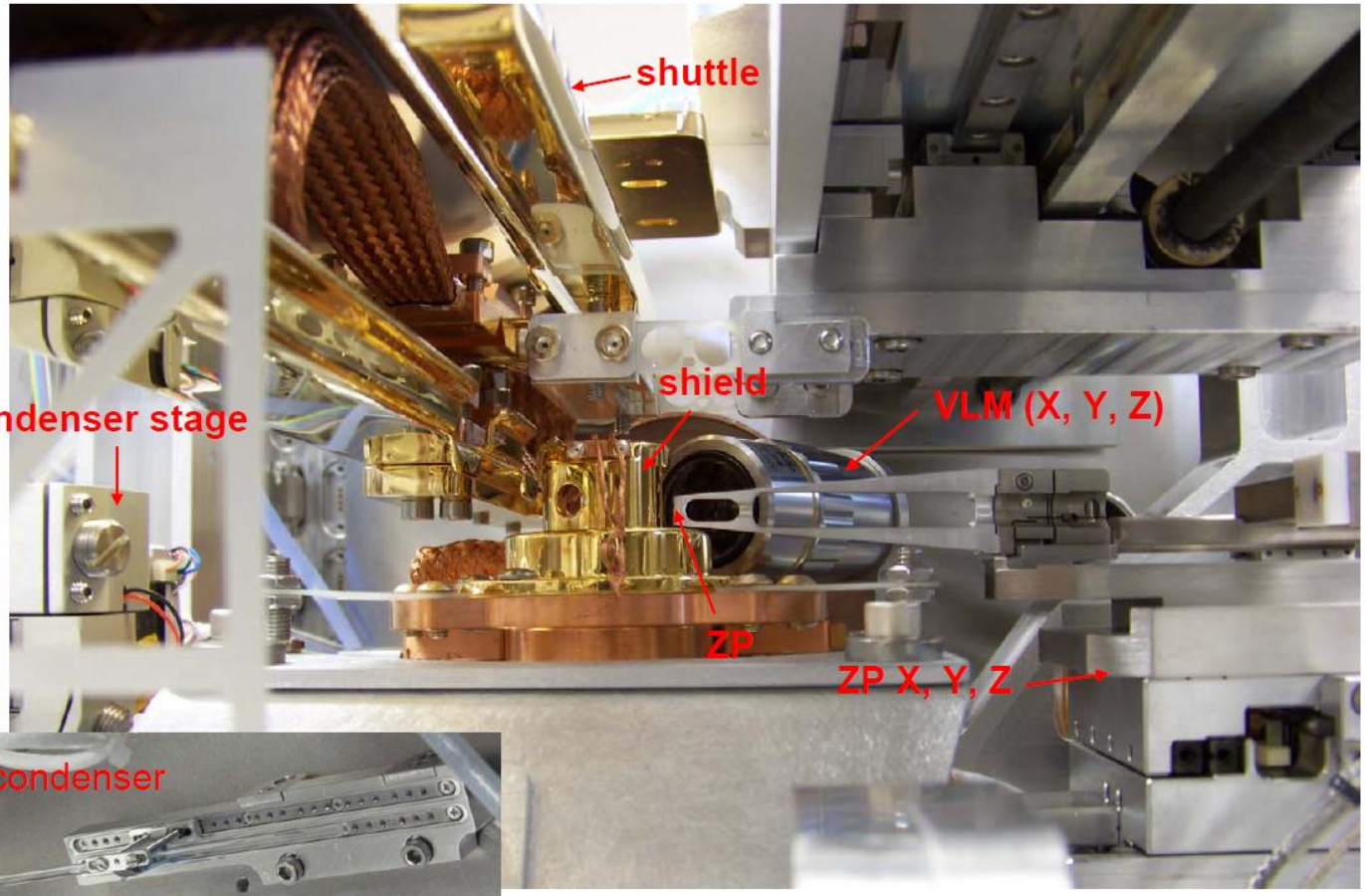

Magnetic layers were fabricated by DC sputtering. Films of 80 nm thickness were grown at rT on top of 50 nm thick silicon nitride windows

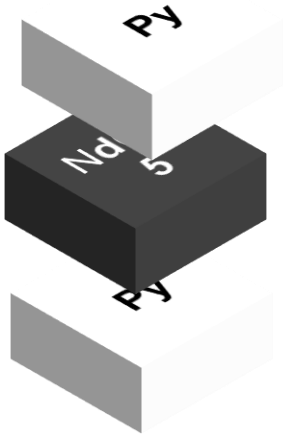

The NdCo5 layer displays weak perpendicular magnetic anisotropy (PMA) leading to magnetic striped domain patterns with canted up and down magnetizations.
The exchange interaction imprints the central striped pattern on the magnetically soft permalloy Ni80Fe20 films

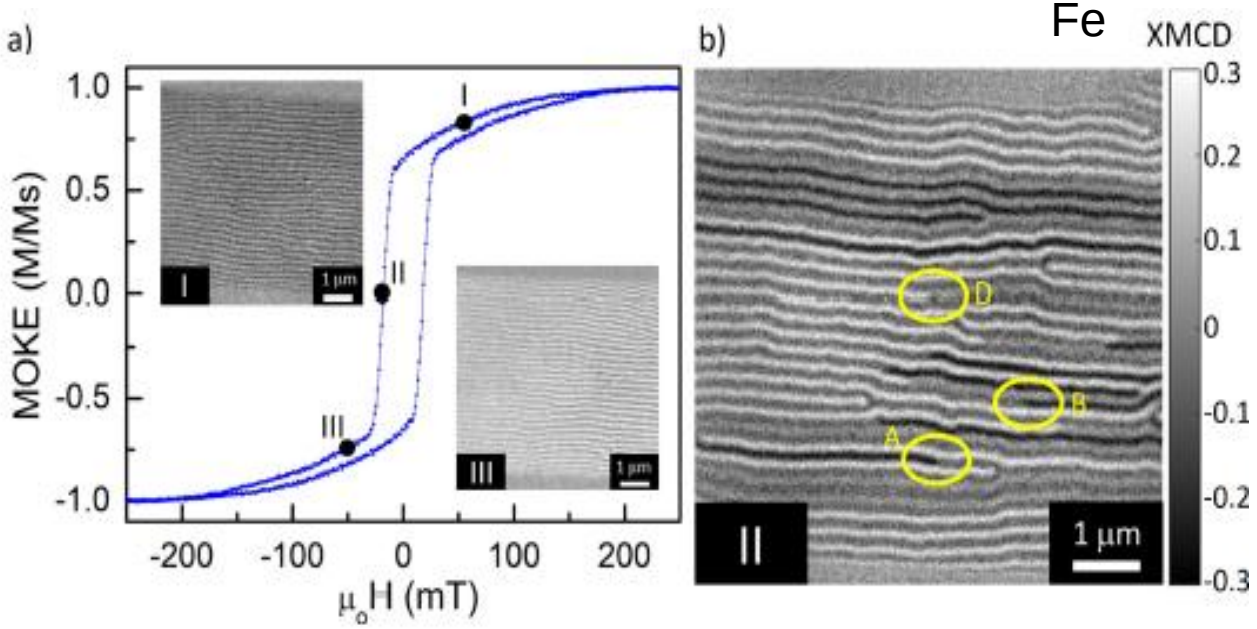

Magnetic imaging

hv = 706.8 eV Fe L_3

k.m

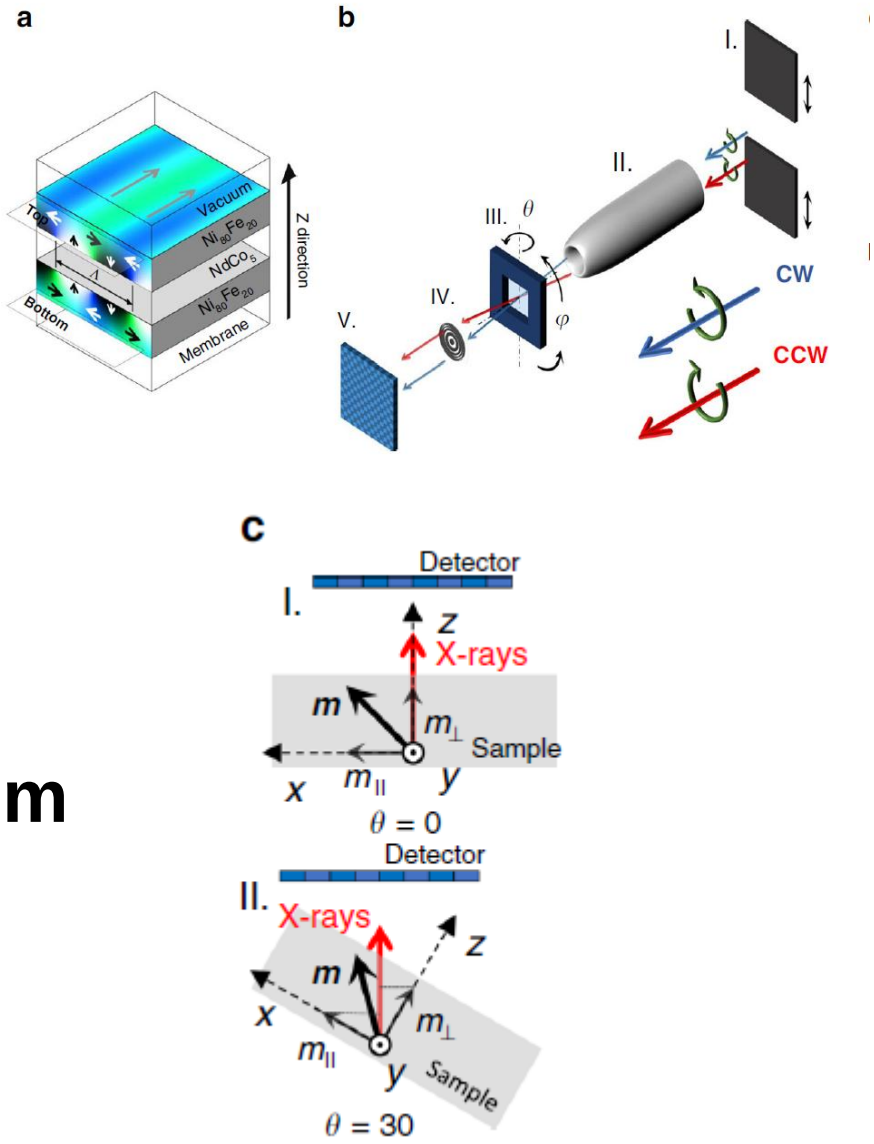

3D Magnetic Vector Imaging

Magnetic Vector Tomography

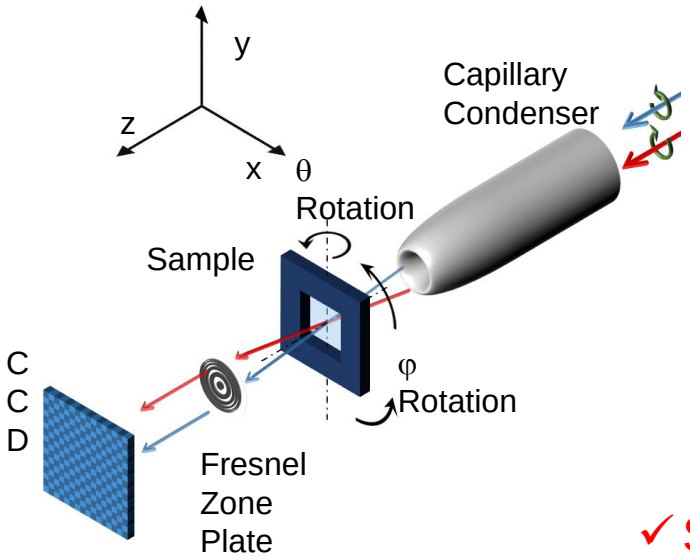

- Dichroic absorption

$$I = I_0 exp\left(-\int_T L^{-1}(t)\left\{1+\delta(t)\left[\vec{k}\cdot\vec{m}(t)\right]\right\}dt\right)$$

L(t) : X ray absorption length
$\delta(t)$ dichroic term, t: thickness
$\vec{k}$: wavector, $\vec{m}(t)$ magnetization

- The acquisition of images with opposite circularly polarized photons allows to separate Structural and Magnetic contributions.

✓ Structural $$\ln\left(\frac{I}{I_0}\right)_{CW} + \ln\left(\frac{I}{I_0}\right)_{CCW} = -2\int_T L^{-1}(t)\,dt$$

✓ Magnetic $$\ln\left(\frac{I}{I_0}\right)_{CW} - \ln\left(\frac{I}{I_0}\right)_{CCW} = -2\int_T L^{-1}(t)\delta(t)\left[\vec{k}\cdot\vec{m}(t)\right]dt$$

Nature Communications **11**, 6382 (2020)

Introduction to tomography

Mathematical Modelling

- No refraction of the incident beams → Accurately Model the Beam path through the object.

Projection at 0 degrees

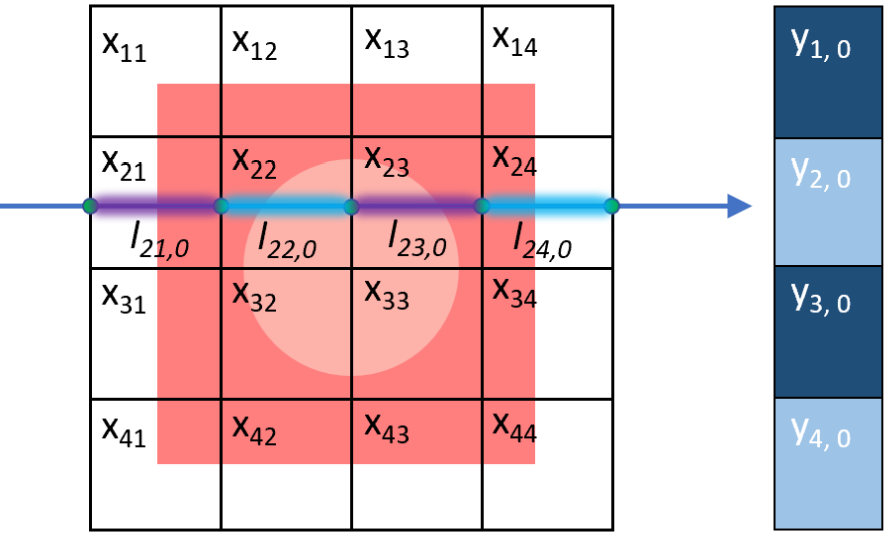

Signal at Pixel y_2 for 0 degrees projection

$$y_{2,0} \propto l_{21,0}x_{21} + l_{22,0}x_{22} + l_{23,0}x_{23} + l_{24,0}x_{24}$$

Introduction to tomography

Mathematical Modelling

- No refraction of the incident beams → Accurately Model the Beam path through the object.

Projection at 30 degrees

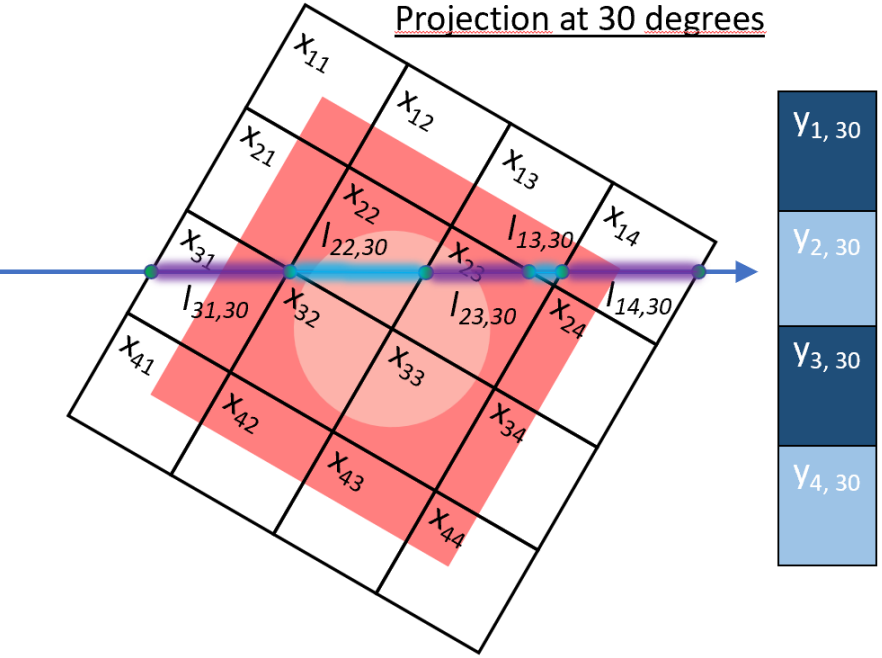

Signal at Pixel y_2 for 0 degrees projection

$$y_{2,0} \propto l_{21,0}x_{21} + l_{22,0}x_{22} + l_{23,0}x_{23} + l_{24,0}x_{24}$$

Signal at Pixel y_2 for 30 degrees projection

$$y_{2,30} \propto l_{31,30}x_{31} + l_{22,30}x_{22} + l_{23,30}x_{23} + l_{13,30}x_{13} + l_{14,30}x_{14}$$

Each detector pixel for each projection gives a linear equation

Introduction to tomography

- This means that we have an equation for each different ray which takes into account different combinations of the model Cells weigthed with the length of the ray path along each specific Cell.

$$y^{\phi} - A^{\phi} x = 0$$

- $y^{\phi}_{n,m}$ → Detector Pixels for a specific Projection.
- A^{ϕ} → Projection Matrix for a specific angle.
- $x_{i,j,k}$ → Model Cells to be projected.

$$y^{\phi} = \begin{bmatrix} y^{\phi}_{1,1} \\ y^{\phi}_{1,2} \\ \vdots \\ y^{\phi}_{n,m} \\ \vdots \\ y^{\phi}_{N,M-1} \\ y^{\phi}_{N,M} \end{bmatrix}, \quad x = \begin{bmatrix} x_{1,1,1} \\ x_{1,2,1} \\ \vdots \\ x_{i,j,k} \\ \vdots \\ x_{I,J-1,K} \\ x_{I,J,K} \end{bmatrix}, \quad A^{\phi} = \begin{bmatrix} l^{1,1,\phi}_{1,1,1} & l^{1,1,\phi}_{1,2,1} & \cdots & l^{1,1,\phi}_{i,j,k} & \cdots & l^{1,1,\phi}_{I,J-1,K} & l^{1,1,\phi}_{I,J,K} \\ l^{1,2,\phi}_{1,1,1} & l^{1,2,\phi}_{1,2,1} & \cdots & l^{1,2,\phi}_{i,i,k} & \cdots & l^{1,2,\phi}_{I,J-1,K} & l^{1,2,\phi}_{I,J,K} \\ \vdots & \vdots & & \vdots & & \vdots & \vdots \\ l^{n,m,\phi}_{1,1,1} & l^{n,m,\phi}_{1,2,1} & \cdots & l^{n,m,\phi}_{i,j,k} & \cdots & l^{n,m,\phi}_{I,J-1,K} & l^{n,m,\phi}_{I,J,K} \\ \vdots & \vdots & & \vdots & & \vdots & \vdots \\ l^{N,M-1,\phi}_{1,1,1} & l^{N,M-1,\phi}_{1,2,1} & \cdots & l^{N,M-1,\phi}_{i,j,k} & \cdots & l^{N,M-1,\phi}_{I,J-1,K} & l^{N,M-1,\phi}_{I,J,K} \\ l^{N,M,\phi}_{1,1,1} & l^{N,M,\phi}_{1,2,1} & \cdots & l^{N,M,\phi}_{i,j,k} & \cdots & l^{N,M,\phi}_{I,J-1,K} & l^{N,M,\phi}_{I,J,K} \end{bmatrix}$$

Introduction to Tomography

- As we are dealing with a huge system of linear equations (256x256 pixels and 100 projections: more than 6,5 million equations), its approximate solution can be found by using an Algebraic Reconstruction Technique (ART).

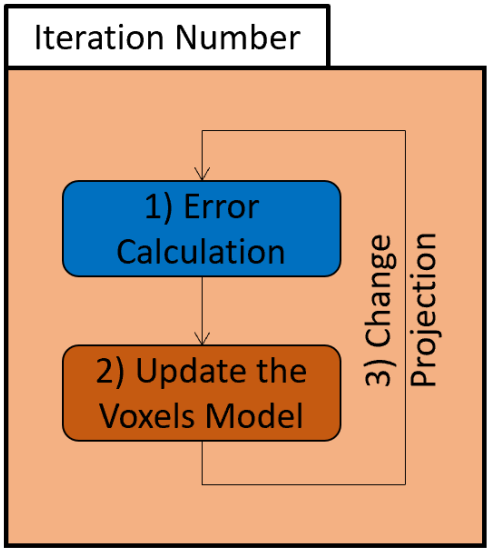

$$1) \quad e^{\phi} = y^{\phi} - A^{\phi} x$$

$$2) \quad x^{new} = x^{old} + \left[C^{\phi} \left[A^{\phi} \right]^{T} R^{\phi} \right] e^{\phi}$$

$$C^{\phi} = \begin{bmatrix} c^{\phi}_{1,1} & 0 & \cdots & & 0 \\ 0 & \ddots & & & \\ \vdots & & c^{\phi}_{c,c} & & \vdots \\ & & & \ddots & 0 \\ 0 & & \cdots & 0 & c^{\phi}_{IJK,IJK} \end{bmatrix}, \quad c^{\phi}_{c,c} = \frac{1}{\sum_{r} l^{\phi}_{r,c}} \qquad R^{\phi} = \begin{bmatrix} r^{\phi}_{1,1} & 0 & \cdots & & 0 \\ 0 & \ddots & & & \\ \vdots & & r^{\phi}_{r,r} & & \vdots \\ & & & \ddots & 0 \\ 0 & & \cdots & 0 & r^{\phi}_{NM,NM} \end{bmatrix}, \quad r^{\phi}_{r,r} = \frac{1}{\sum_{c} l^{\phi}_{r,c}}$$

J. Synchrotron Rad. (2018). ***25,*** *1144-1152*

J. Synchrotron Rad. (2025). **32**, 1095–1104

- Experimental demonstration of the method in a magnetic heterostructure with weak PMA. $Ni_{80}Fe_{20}$(80nm)/$NdCo_5$(80nm)/$Ni_{80}Fe_{20}$(80nm)

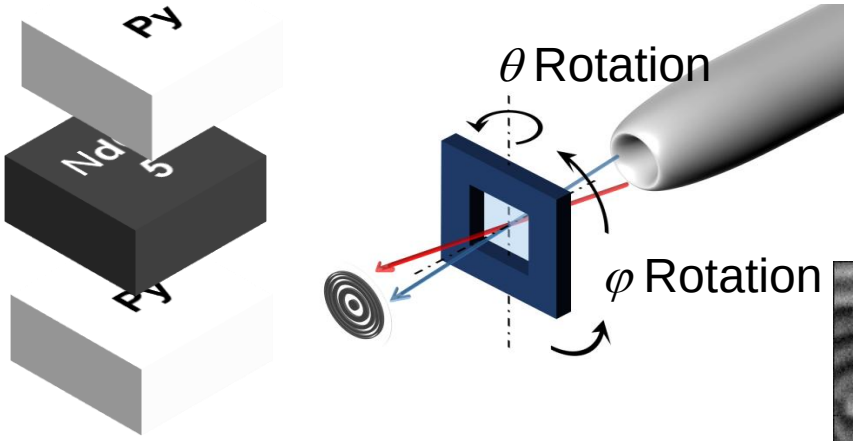

Magnetic Tilt series 1
$\varphi = 0°$

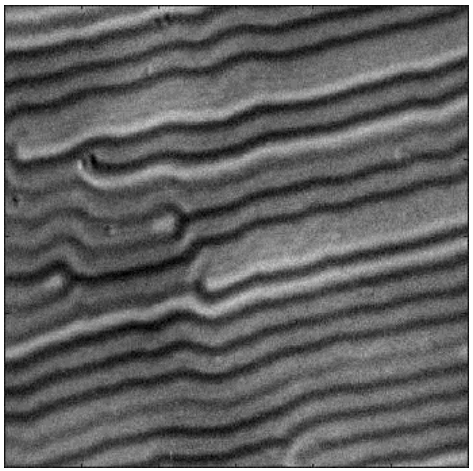

Magnetic Tilt series 2
$\varphi = 102°$

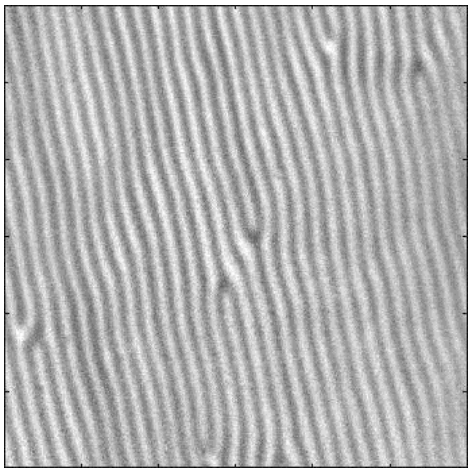

✓ In-plane reversal initiated.

✓ Measurements at Fe L_3 edge with C+ and C- circular polarizations from $\theta = -55°$ to $\theta = 55°$.

✓ Two Tilt series recorded for $\varphi = 0°$ and $\varphi = 102°$

Nature Communications **11**, 6382 (2020)

Results

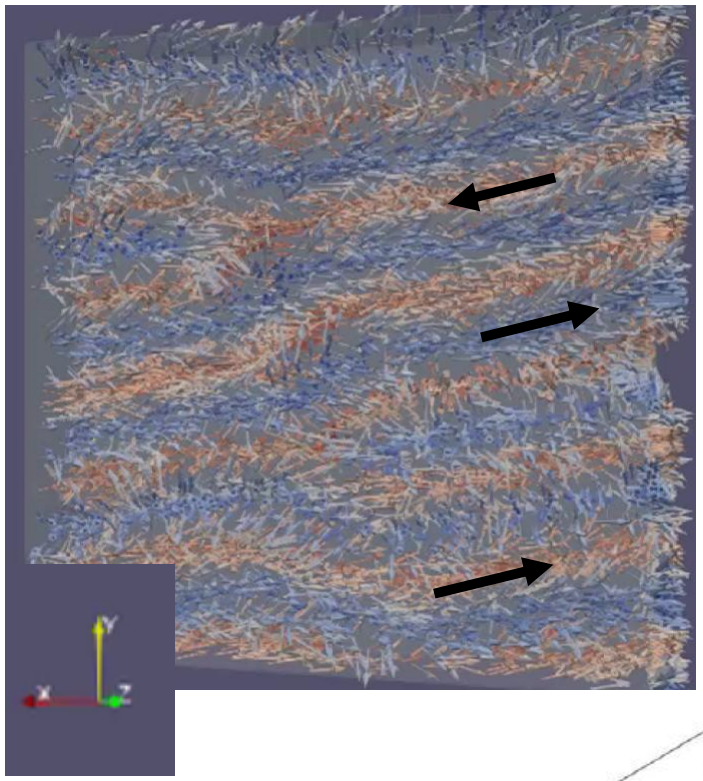

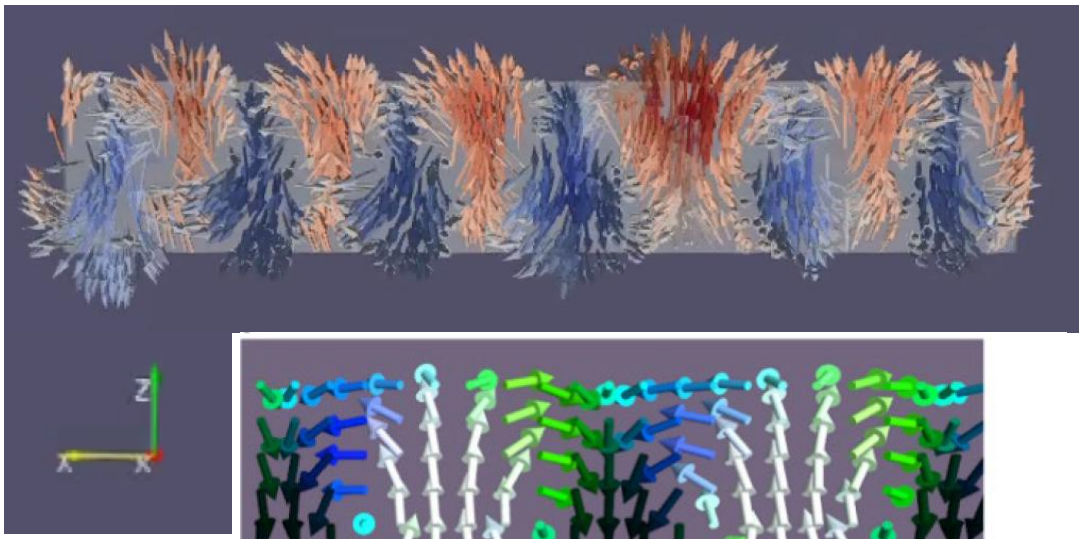
z
x

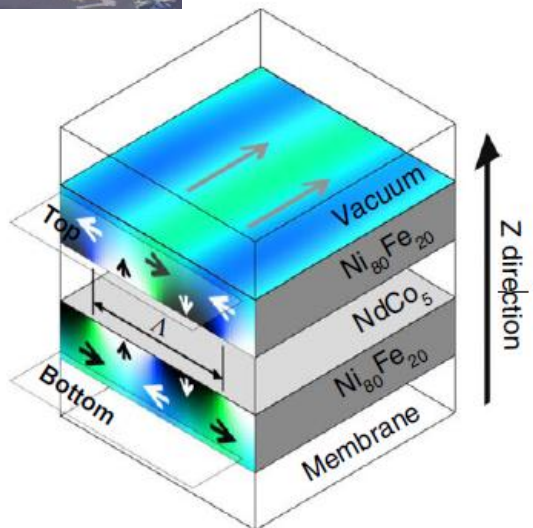
Top
Vacuum
$Ni_{80}Fe_{20}$
$NdCo_5$
$Ni_{80}Fe_{20}$
Membrane
Bottom
Λ
Z direction

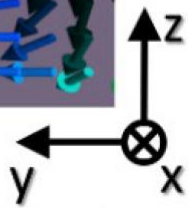
z
y
x

Magnetic singularities

2D

skyrmion

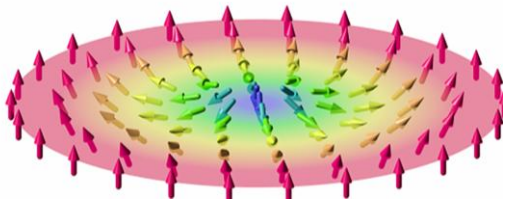

meron

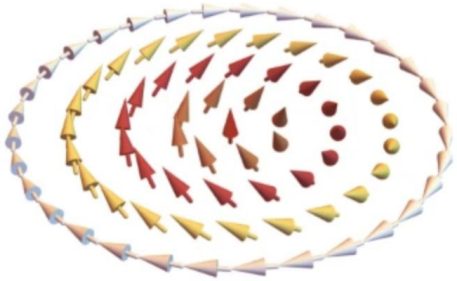

anti vortex

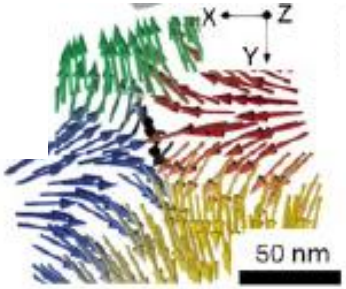

vortex

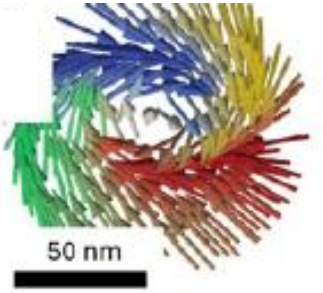

3D

Bloch points (m= 0)

radial

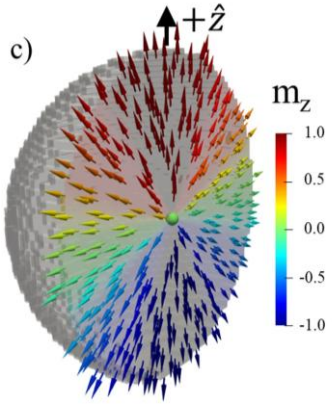

axial
tail to tail

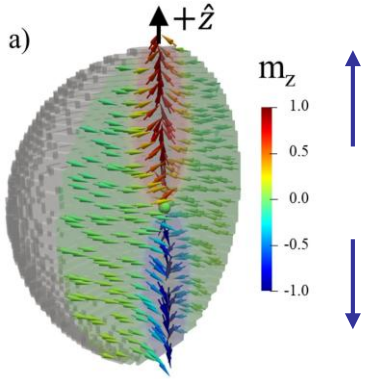

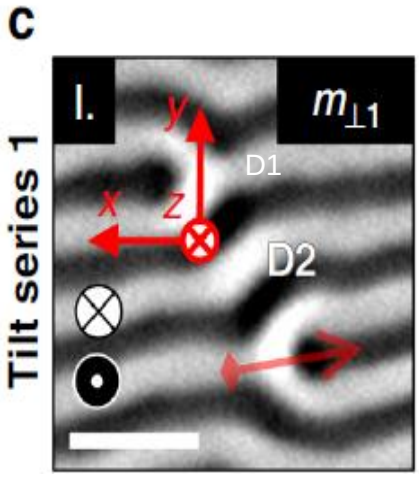

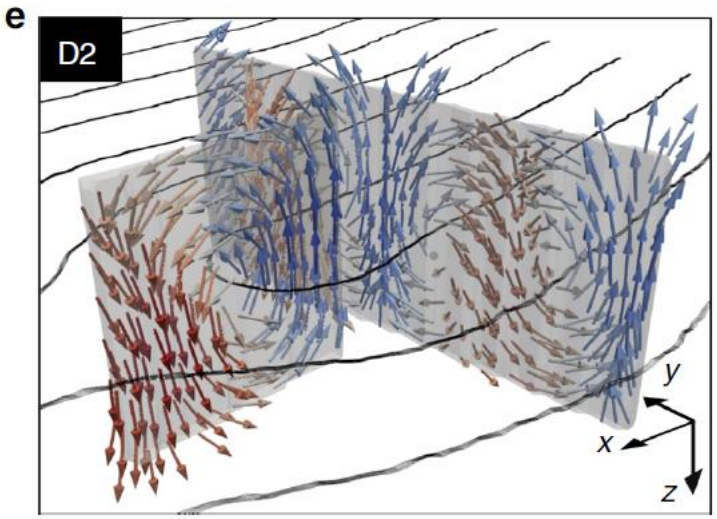

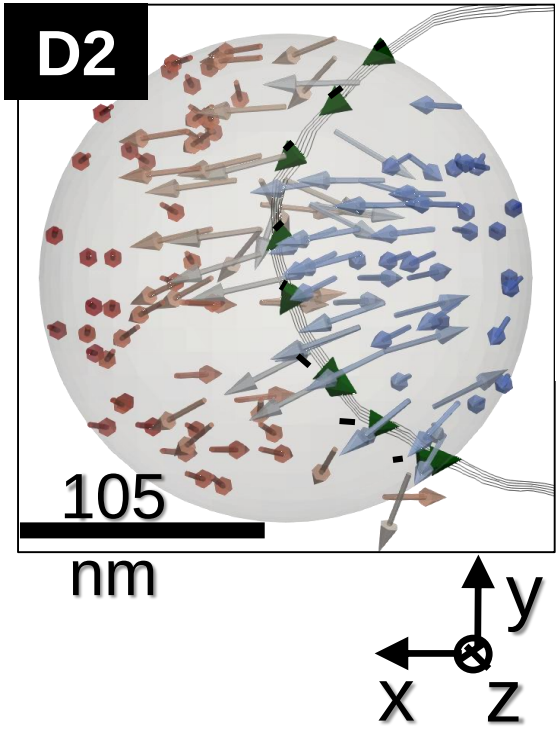

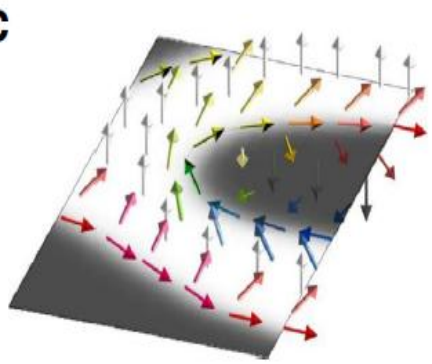

meron-like

3D

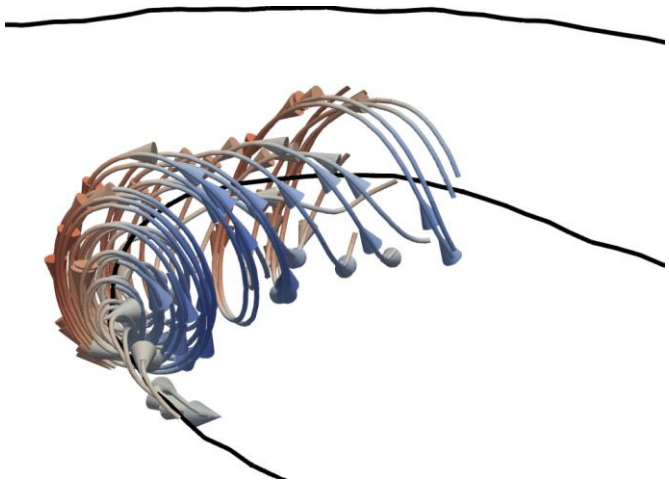

Topological charges

Magnetic singularities are characterized by their topological charges

In 2D systems as

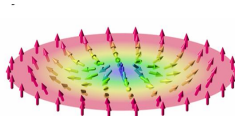

$$Q_{top}^{2D} = \frac{1}{4\pi}\int \vec{m}\cdot\left(\partial_x\vec{m}\times\partial_y\vec{m}\right)dS_z$$

2D Topological Charge Density

In 3D systems $Q_{top} = \frac{1}{8\pi}\int \epsilon_{i,j,k}\vec{m}\cdot\left(\partial_j\vec{m}\times\partial_k\vec{m}\right)dS_i \propto \int B_i dS_i$ *i,j,k= x,y,z*

$$\boldsymbol{B_e} \propto \left[\boldsymbol{m}\cdot\left(\frac{\partial \boldsymbol{m}}{\partial y}\times\frac{\partial \boldsymbol{m}}{\partial z}\right), \boldsymbol{m}\cdot\left(\frac{\partial \boldsymbol{m}}{\partial z}\times\frac{\partial \boldsymbol{m}}{\partial x}\right), \boldsymbol{m}\cdot\left(\frac{\partial \boldsymbol{m}}{\partial x}\times\frac{\partial \boldsymbol{m}}{\partial y}\right)\right]$$

emergent magnetic field

Be is a ¨real¨ field: topological Hall effect

vx**B**e

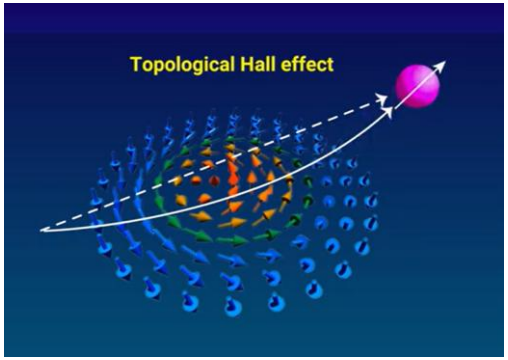

Magnetic singularities

2D

skyrmion

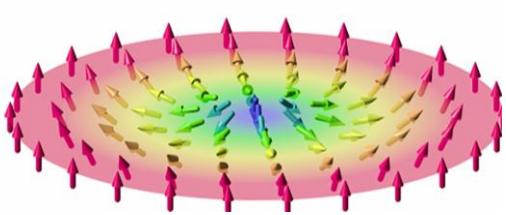

Q=1

meron

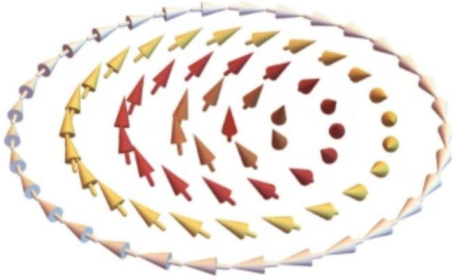

Q= 1/2

anti vortex

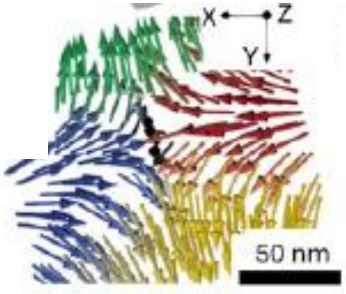

Q= -1/2

vortex

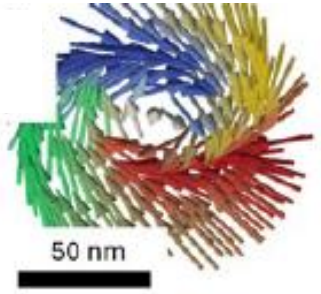

Q= 1/2

3D

Bloch points

radial

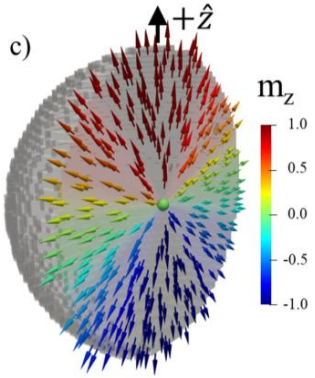

Q=1

axial
tail to tail

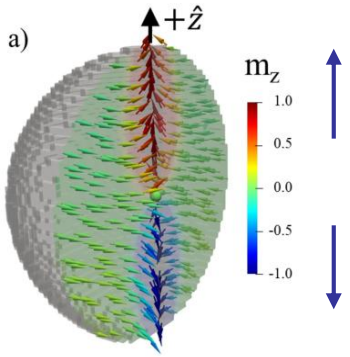

Q= -1

Emergent field of the Bloch point in Py/GdCo/ Py trilayer

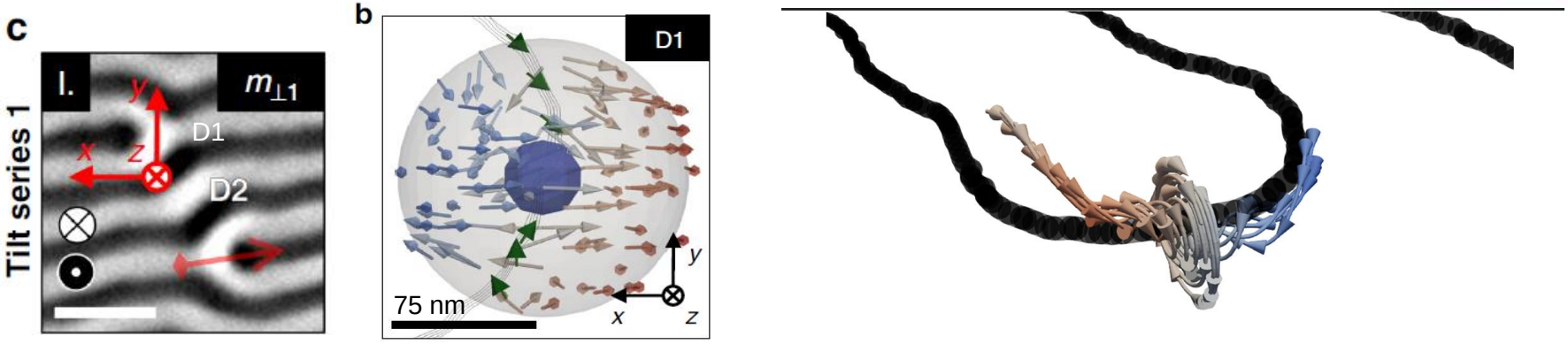

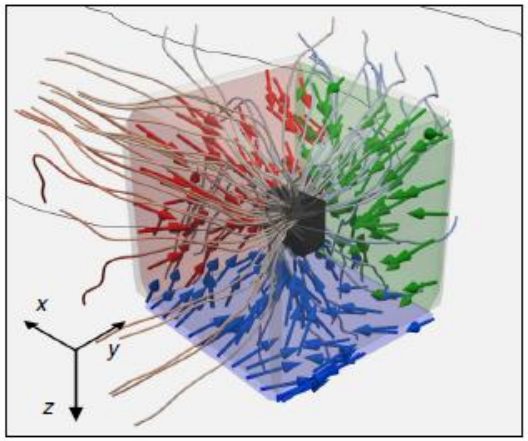

streamlines and arrows of emergent field obtained numerically from our reconstructed magnetization data around the Bloch point

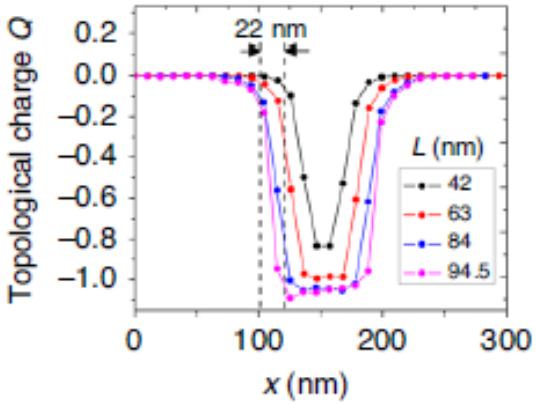

profile of the total topological charge Q obtained integrating over cubes of different side dimensions. The precision on the localization of the Bloch point is ca. 22 nm

More on Bloch points : pure permalloy sample

140 nm thick sample on Si_3N_4 fabricated by e-beam lithography, DC magnetron sputtering and liftoff

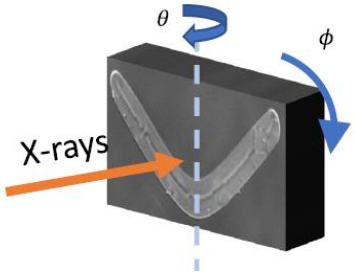

θ from -55 to 55 steps of 1 or 2 deg.

φ = 0

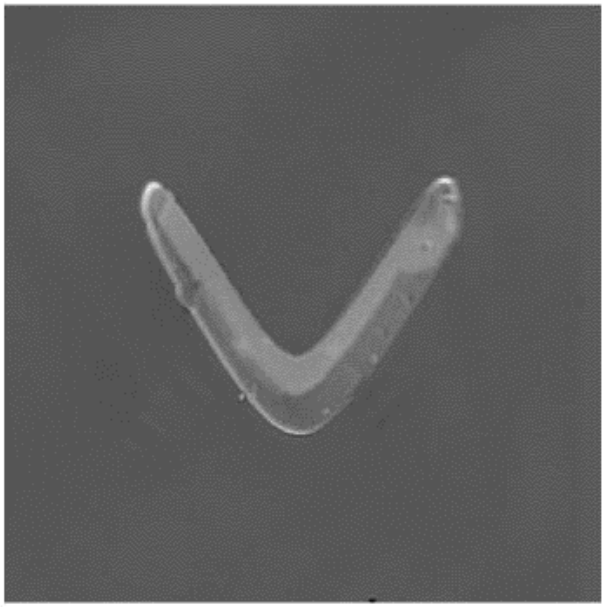

φ = 90

Central plane of the sample from tomographic reconstruction

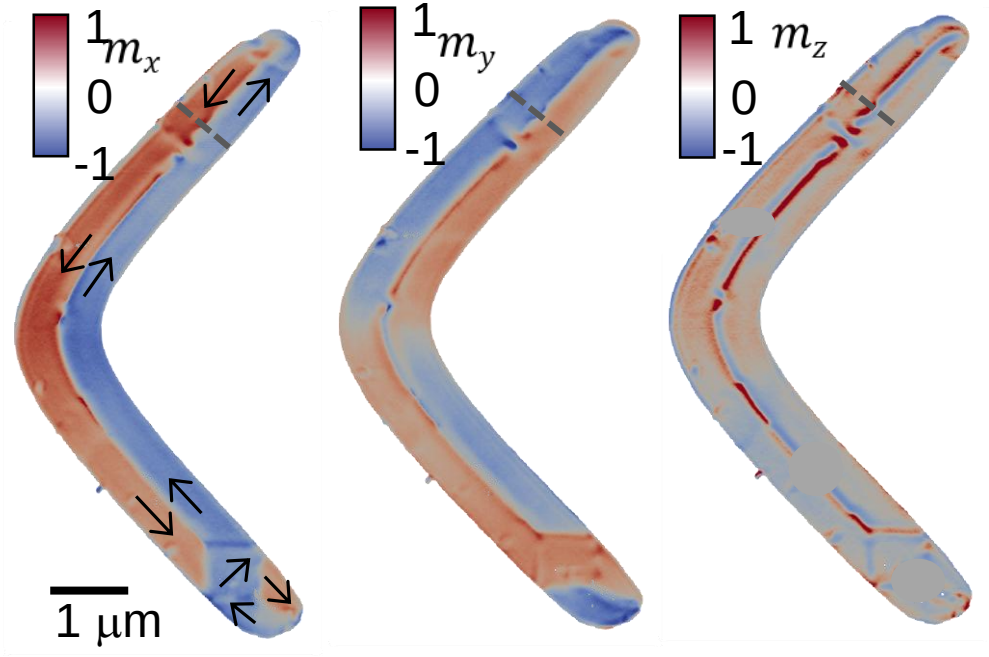

commun. Phys. **6**, 49 (2023)

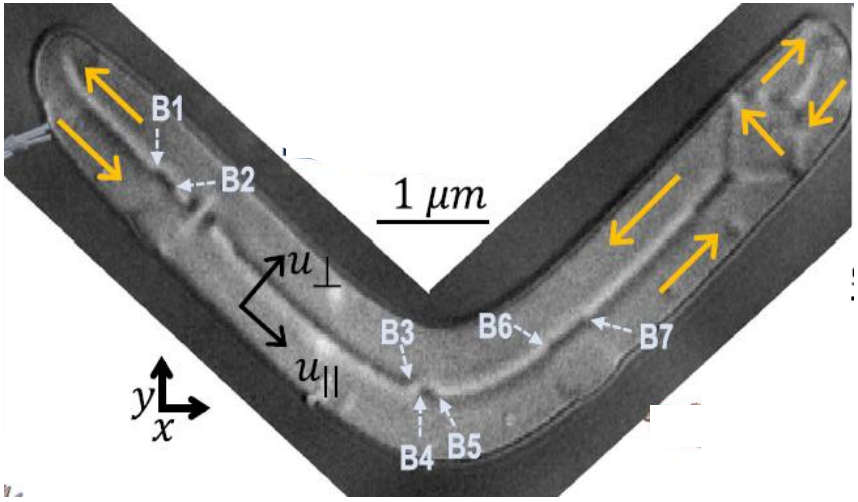

Bloch Points decorating the domain wall at the center of the structure.

Pairs of Bloch points with opposite charge

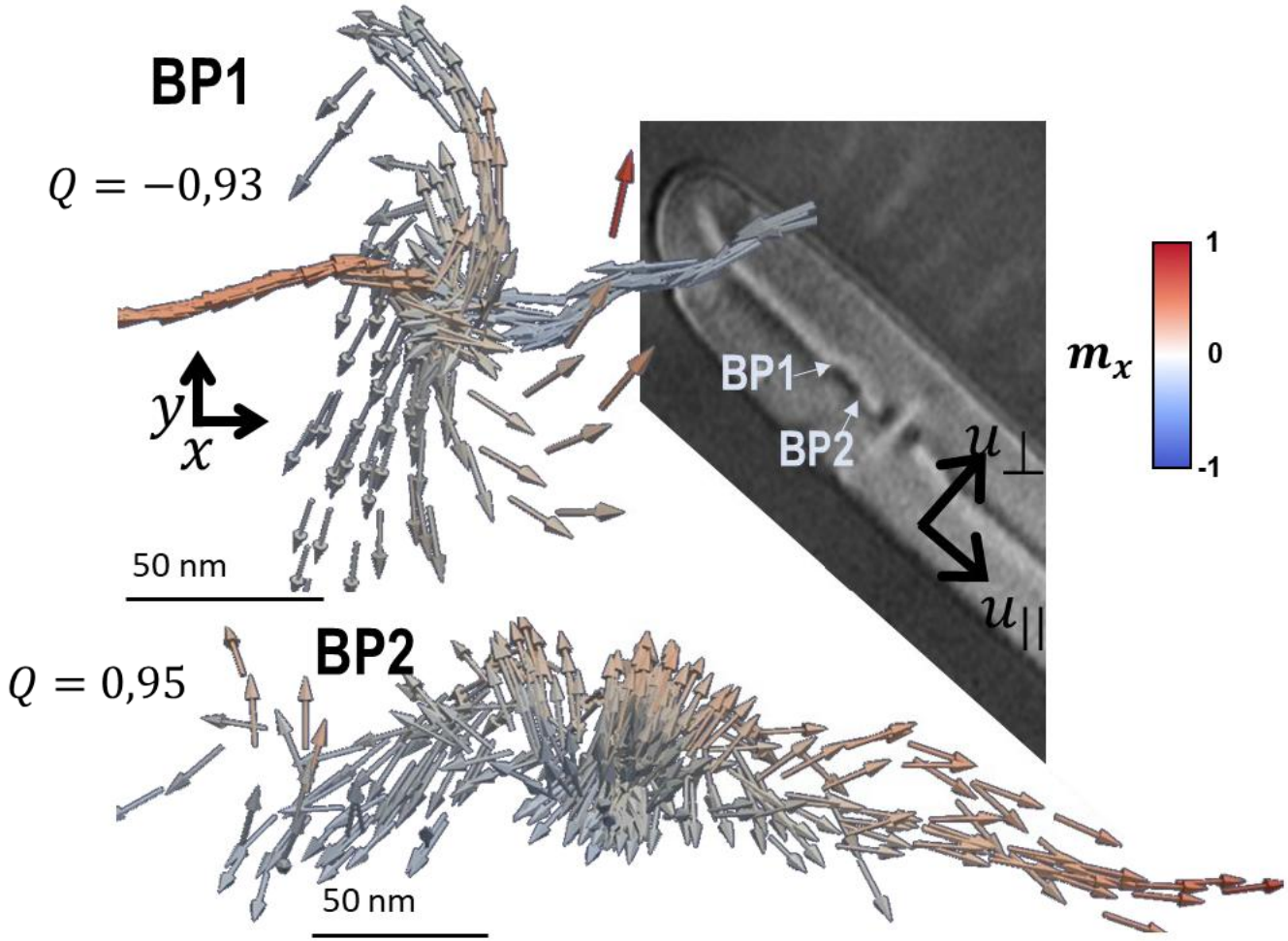

Pairs of Bloch points with opposite charge

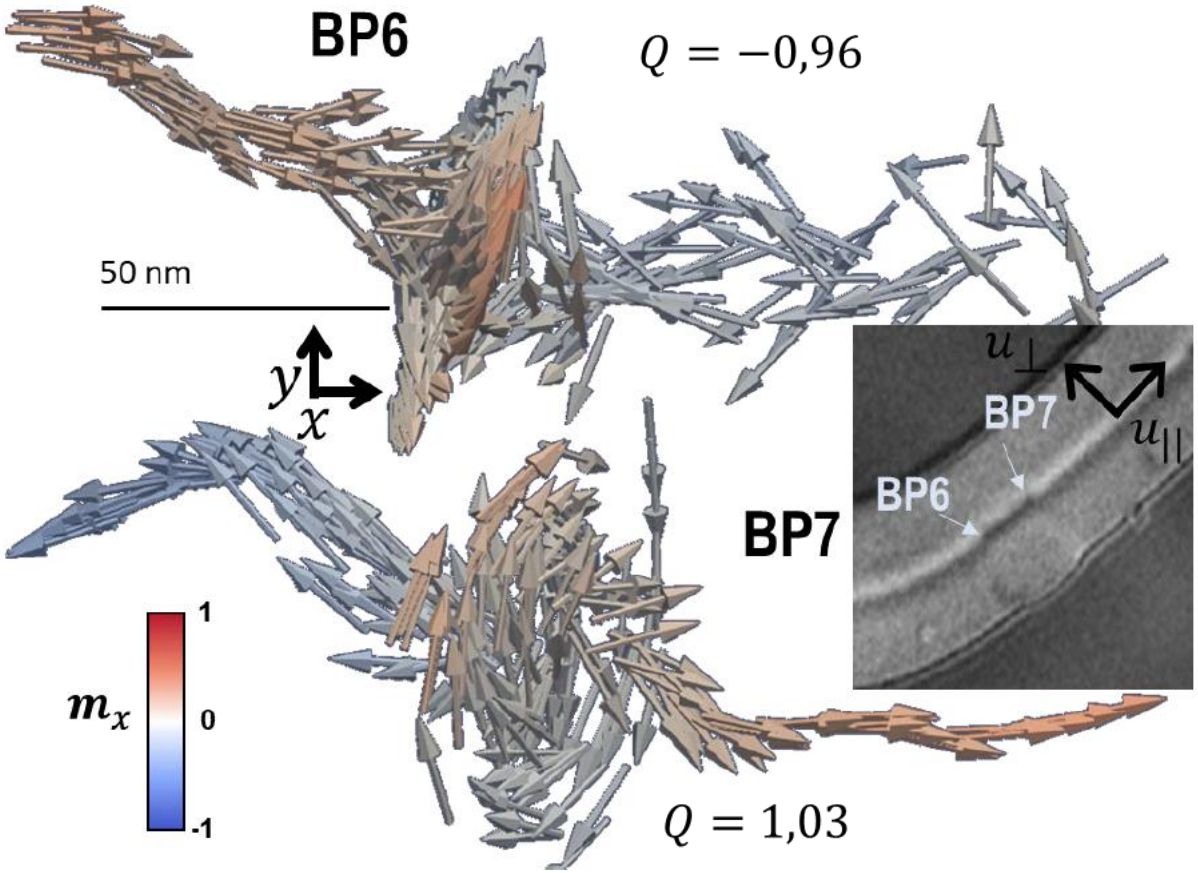

Emergent field near BP6 (Q= -1)

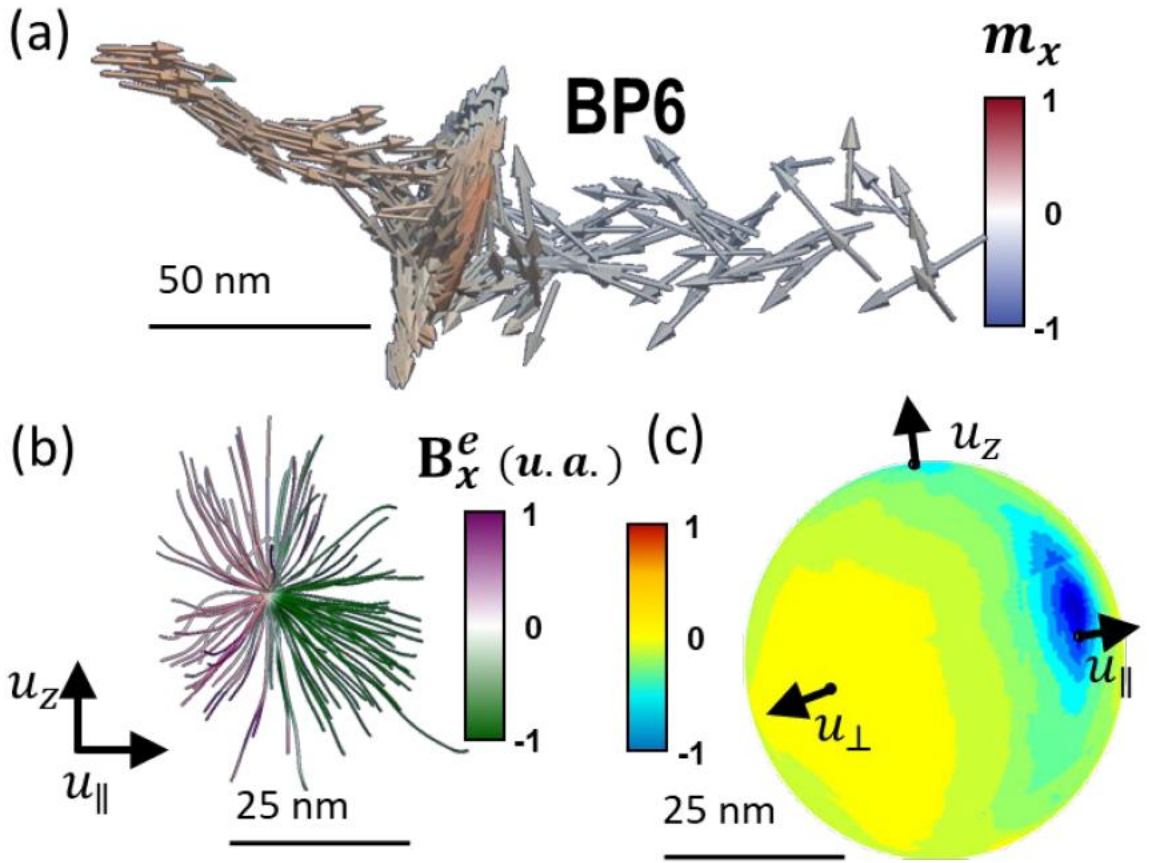

Extended emergent field

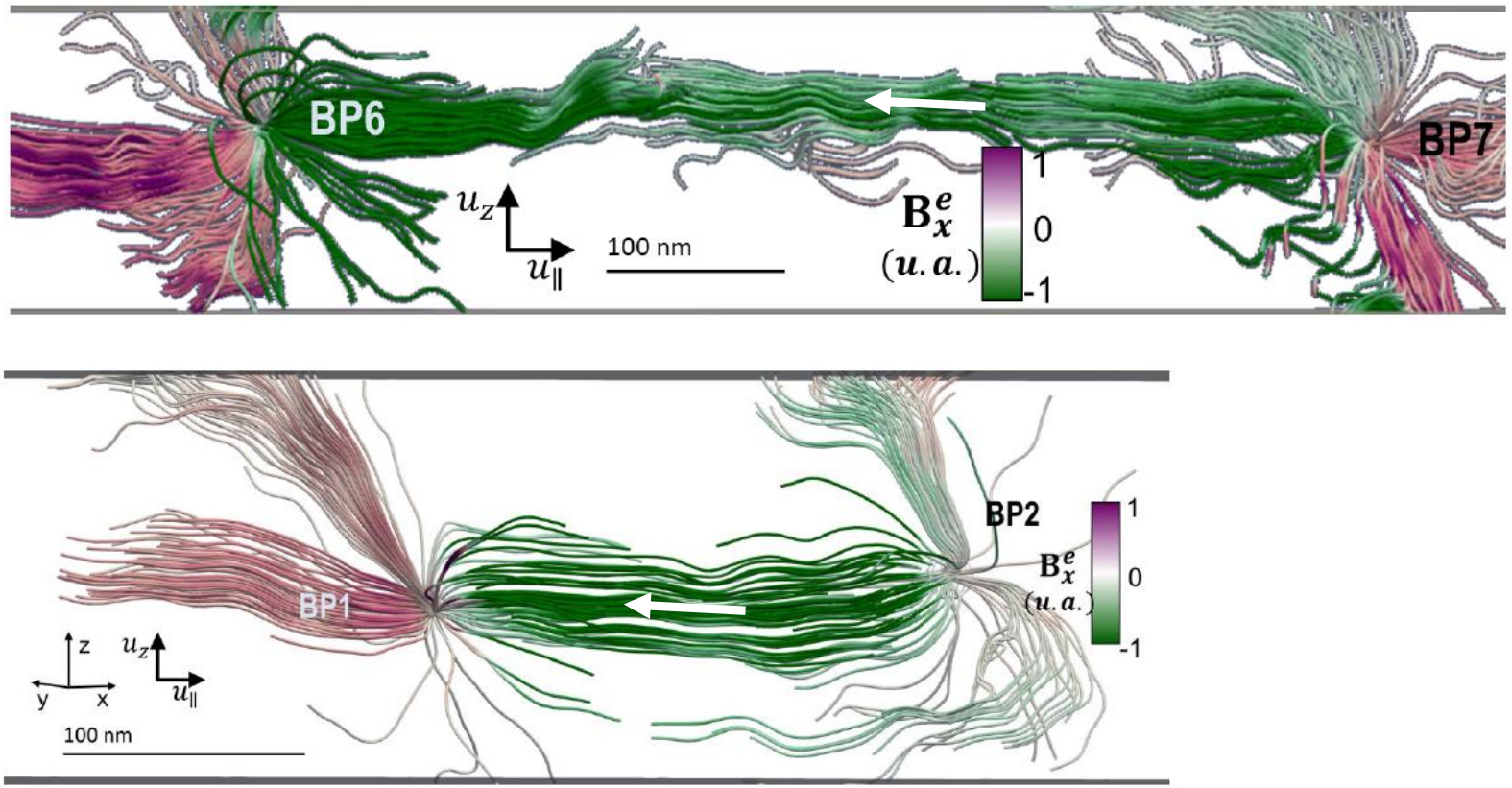

- Opposite topological charge Bloch Points are connected via $\boldsymbol{B_e}$ lines.

- At larger scales the radial simmetry is distorted by the magnetization configuration. The larger flux of $\boldsymbol{B_e}$ is at the core of the central domain wall.

Triplets B3, B4 and B5

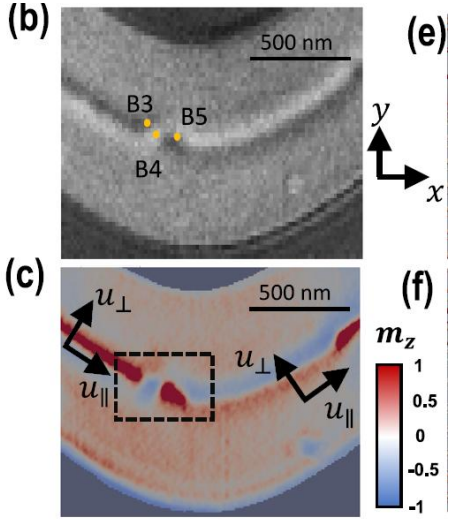

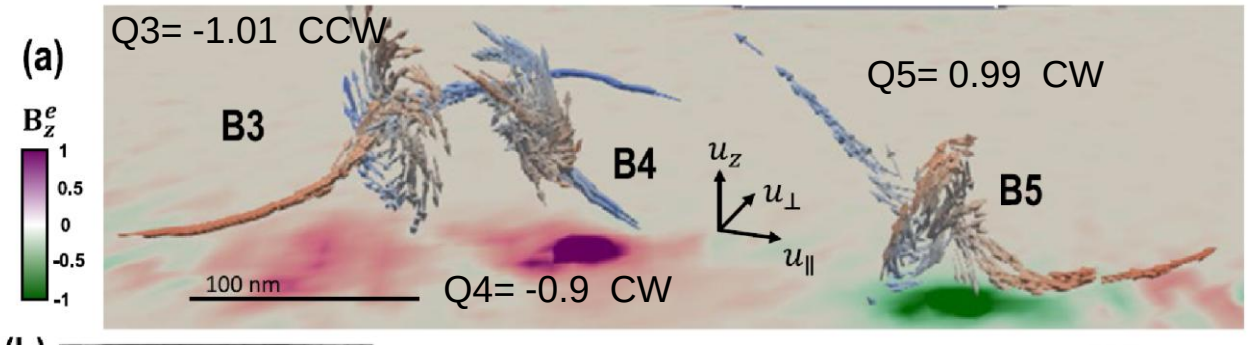

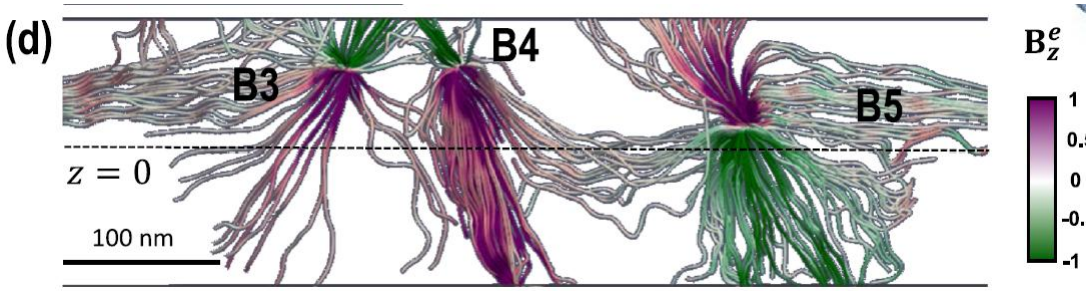

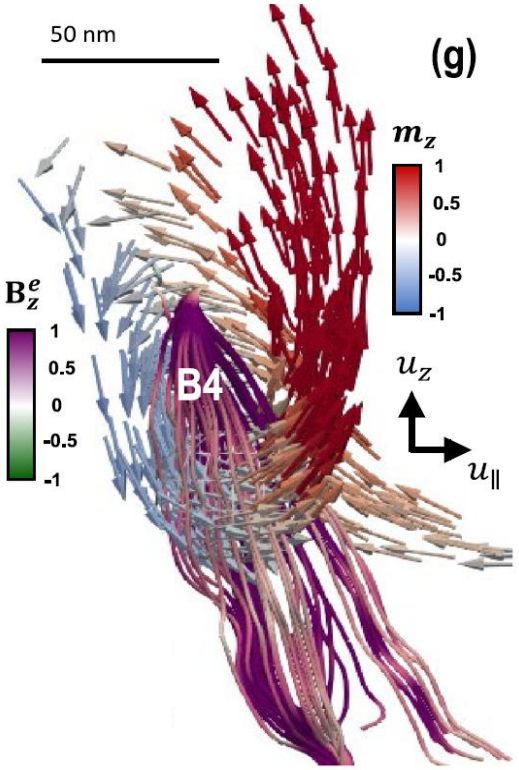

Hyperbolic Bloch points in ferrimagnetic exchange spring

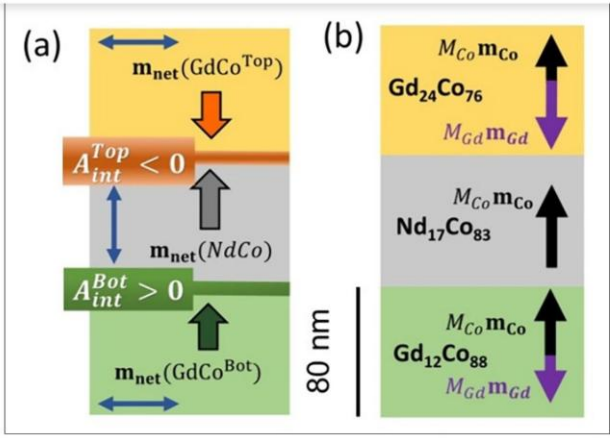

X-ray magnetic circular dichroism at the Gd M4 (1221.9 eV) and Gd M5 (1189.6 eV)

Bloch points

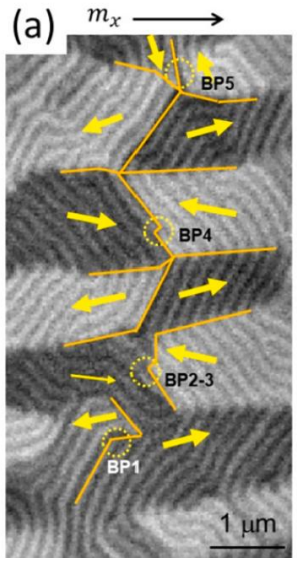

hyperbolic

circulating

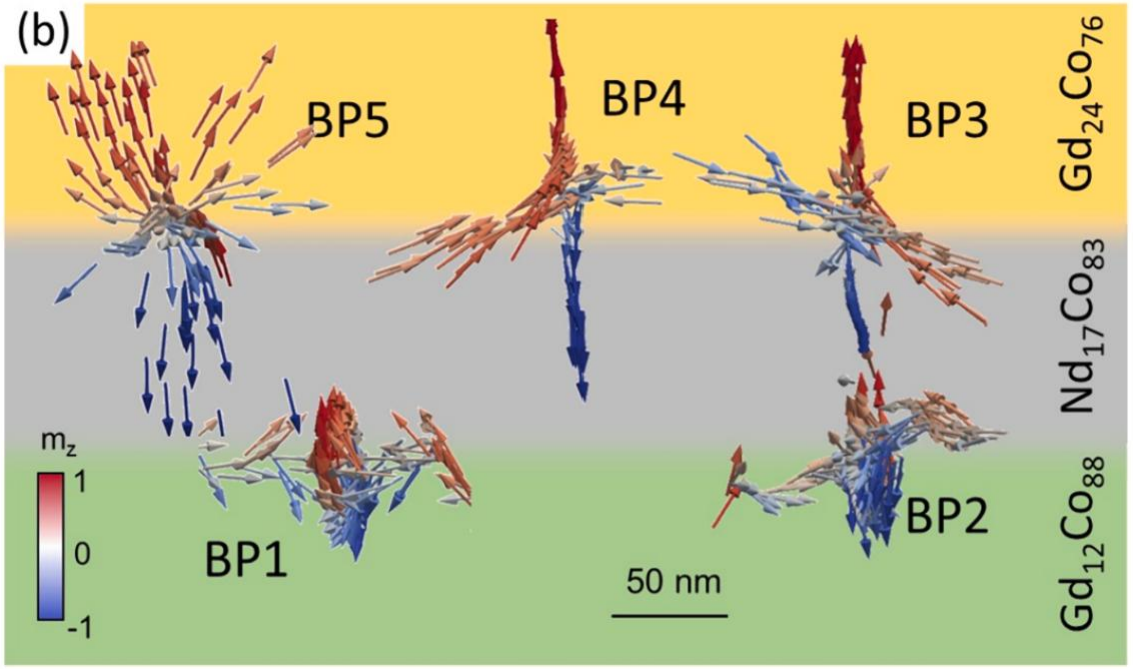

Results in Physics 61 (2024) 107771

Conclusions

- Jumping to 3D geometries and not restricting the magnetization configuration dimensionality enriches the magnetization vector field. 3D Nanomagnetism is a Paradigm change!

- The challenge of experimentally visualizing in 3D the magnetization can be resolved via magnetic vector tomography.

- Magnetic vector tomography is a **purely experimental approach** for vector characterization of the magnetization with no prior assumptions, paving the way to Experimental Micromagnetism.

- Topology can be a very useful tool to help in the analysis and understanding of complex and extended magnetization systems allowing to identify interesting textures and to further comprehend magnetization processes

How pure is the circular polarization at Mistral ?

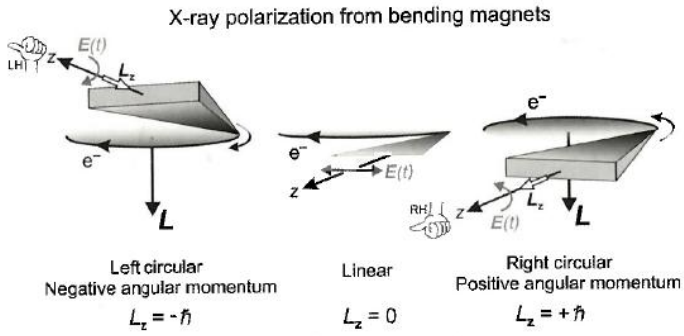

Present situation:

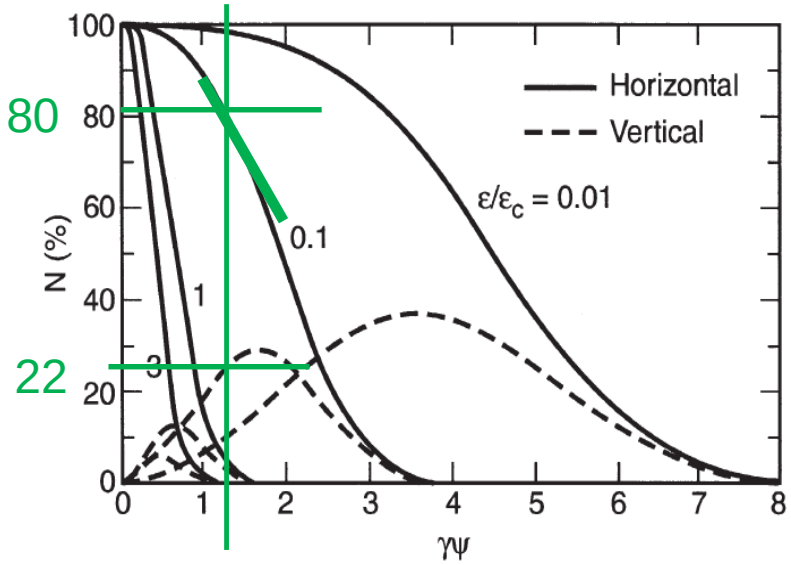

Fig. 2-2. Normalized intensities of horizontal and vertical polarization components, as functions of the vertical observation angle ψ, for different photon energies. (Adapted from Ref. 1.)

γ = electron energy/$m_e c^2$

ε/εc for **Co L3** = 0.149
ψ= aprox 200 μrad
γψ = 1.17

Mistral operation with circular polarization is approx 80% horizontal and 20 % vertical intensities , which corresponds to an elliptical polarization that may be described as the superposition of H polarization plus circular polarization with the same amplitudes

Hor pol = A **x** cosθ (θ=ωt)

Circ pol = A(**x** cos θ + **y** sin θ)

Same amplitude, same intensity

50% Hor + 50 % Circ

Elliptical polarization

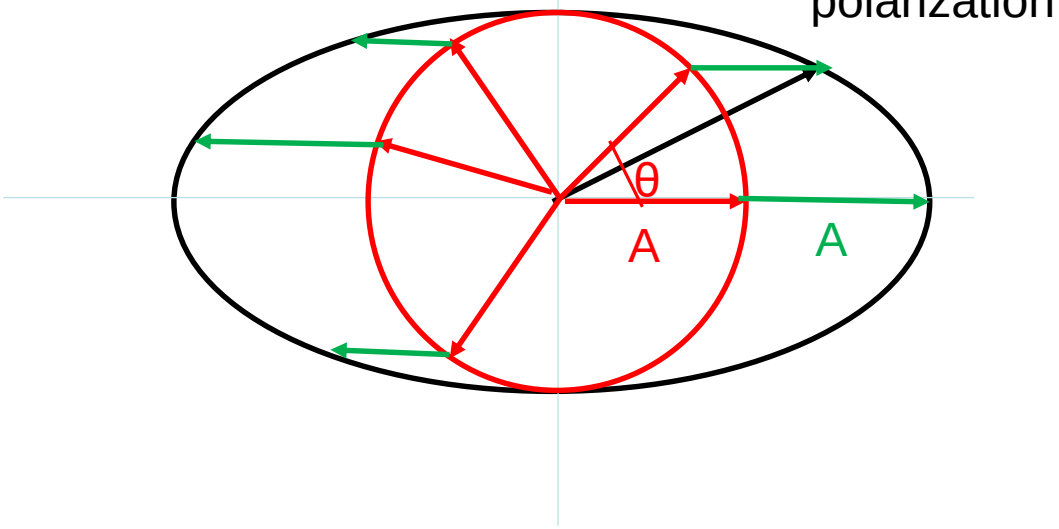

BOREAS: helical undulator

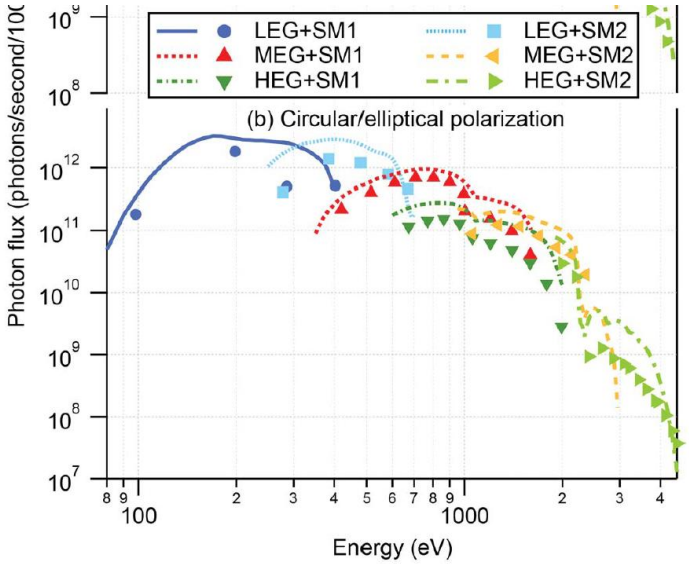

Figure 9
Measured (symbols) and calculated (lines) flux at the sample, with ES and XS opening of 15 µm and 100 mA electron beam current, for (*a*) linear polarization and (*b*) circular (up to 1100 eV) or elliptical (above 1100 eV) polarization.

MISTRAL: bending mag

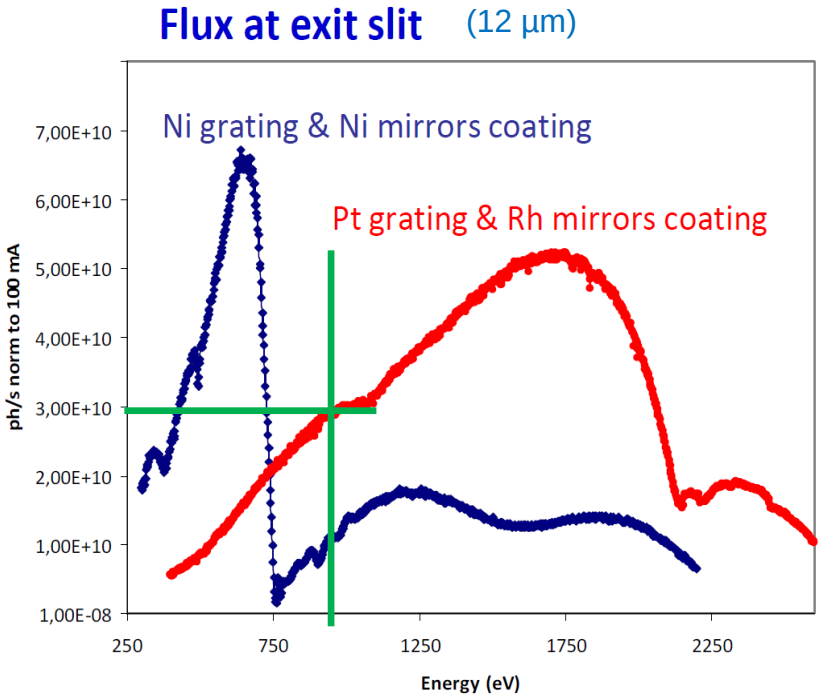

Flux at 900 eV about $3x10^{10}$ ph/s

$3x10^{10}$ x 0.5 (circular) = $1.5x10^{10}$

900 eV : 10^{12} ph/s circular polarization

100 % polarization circular

10^{12}/ $1.5x10^{10}$ ≈ 67

Tilt angular series: from 10 hours to ~ 9 minutes and no background

The cast

Universidad de Oviedo

María Vélez
Aurelio Hierro
José Ignacio Martín
Luis Manuel Álvarez-Prado
Carlos Quirós
Javier Hermosa-Muñoz
Alicia Estela Herguedas-Alonso
Victoria Vega Fernandez

ALBA

Eva Pereiro
Andrea Sorrentino
Claudia Fernández-González
Lucia Aballe
Sandra Ruiz-Gomez
Ricardo Valcárcel
Josep Nicolas
Zeus Martí

Thanks for listening